Electronic Supplementary Material (ESI) for Inorganic Chemistry Frontiers.
This journal is © the Partner Organisations 2021

Supplementary information for

Solvent assisted delamination of the layered copper dithienothiophene-dicarboxylate (DUT-134)

Friedrich Schwotzer, Irena Senkovska*, Volodymyr Bon, Stefanie Lochmann, Jack D. Evans, Darius Pohl, Bernd Rellinghaus, and Stefan Kaskel*

1. Methods and Materials 2
2. Physical Measurements 3
3. Experimental data 4
4. Theoretical calculations 5
5. Detailed crystallographic data 6
6. Crystal structure of the dithieno[3,2-b:2',3'-d]thiophene-2,6-dicarboxylic acid (H_2DTTC) 11
7. Optical and SEM images 12
8. Comparison of different activation methods 12
9. High-resolution TEM measurements 13
10. Adsorption isotherms 14
11. Zeo++ Calculations[3] 17
12. In situ PXRD during *n*-butane adsorption at 273 K 19
13. Ex situ PXRD during EtOH adsorption at 298 K 20
14. Exfoliation 21
15. Thermogravimetric analysis 22
16. Infrared (IR) and Raman spectroscopy 23
17. NMR spectroscopy 24

1. Methods and Materials

Materials. All the reagents and solvents for synthesis were purchased from commercial sources and used as supplied without further purification.

Supplementary Table 1: List of chemicals used for the synthesis of ligands and MOFs.

Name	**CAS**	**purity**	**Manufacturer**
1-Formylpiperidine	2591-86-8	>98%	TCI
1-Propanol	71-23-8	100 %	VWR Chemicals
2-Heptanone	110-43-0	>98%	TCI
2-Pentanone	107-87-9	≥99.5%	Sigma Aldrich
2-Propanol	67-63-0	100.0%	VWR Chemicals
Acetone	67-64-1	≥99.8%, extra dry	Fisher Scientific
Acetonitrile	75-05-8	≥99.5%	Sigma Aldrich
Butanone	78-93-3	≥99%	AppliChem
Copper(II) nitrate trihydrate	10031-43-3	98%	Sigma Aldrich
Dichlormethane (DCM)	75-09-2	≥99.8	Sigma Aldrich
Ethanol	64-17-5	≥99.8	Sigma Aldrich
Ethyl thioglycolate	623-51-8	97%	Sigma Aldrich
Hydrochloric acid	7647-01-0	37%	Sigma Aldrich
Lithium hydroxide	1310-65-2	98%	Sigma Aldrich
Methanol	67-56-1	≥99.9%	Sigma Aldrich
Methyl sulfoxide	67-68-5	≥99.8%, extra dry	Fisher Scientific
n-Butyllithium	109-72-8	2.5 M in hexanes	Sigma Aldrich
N,*N*-Dimethylformamide (DMF)	68-12-2	≥99.8%, extra dry	Fisher Scientific
Potassium carbonate	584-08-7	≥99%	Sigma Aldrich
Tetrabromothiophene	3958-03-0	>99%	TCI
Tetrahydrofuran (THF)	109-99-9	≥99.9, anhydrous	Sigma Aldrich
Toluene	108-88-3	99.9%	VWR Chemicals

2. Physical Measurements

Scanning electron microscopy (SEM) measurements were carried out using a 2 kV acceleration voltage and a working distance of 12 mm on a SU8020 from Hitachi. Prior to the measurements, the samples were sputtered with Au to increase the conductivity. EDX was performed on the same instrument using a working distance of 15 mm and an acceleration voltage of 20 kV. PXRD experiments at room temperature were carried out on an STOE STADI P diffractometer with Cu Kα1 radiation (λ = 1.5405 Å) and a 2D detector (Mythen, Dectris) in transmission geometry. Thermogravimetric (TGA) analysis was recorded on a NETZSCH STA 409 thermal analyser at a heating rate of 5 K min^{-1} in synthetic dry air. Air sensitive MOF samples were prepared in an Ar-filled glovebox and inserted in the instrument with minimum exposure to ambient conditions. Elemental analysis experiments were performed on a HEKAtech EA 3000 Euro Vector CHNSO Elementaranalysator in CHNS modus. The composition was determined as the average of three individual measurements on three individually prepared samples. Guest free powder of DUT-134 was analysed by placing 3 - 5 mg of sample in Sn-sample holders under an inert atmosphere in a glove box and sealed to avoid contamination with humidity. The measurement of the layer thickness was performed on the atomic force microscope (AFM) Dimension D 3000 from Digital Instruments (Bruker) in tapping mode with a measuring speed of 2 - 5 µm/s. Diffuse reflectance infrared Fourier transform (DRIFT) spectra of organic linker and intermediates were measured on a BRUKER VERTEX 70 with a SPECAC Golden Gate DRIFT setup. Prior to the measurement 2 mg of the sample were mixed with 100 mg dry KBr in a mortar and pressed to a pellet. MOF samples were handled in an Ar-filled glovebox. The Raman measurements were performed with the Confocal Raman Microscope (CRS+) MonoVista from Spectroscopy & Imaging GmbH using lasers with wavelengths of 514 nm and 785 nm. Supercritical dried samples were measured under inert conditions (Ar atmosphere) in quartz glass fluorescence cuvettes (1 mm path length). Transmission electron microscopy measurements have been conducted using a JEOL JEM F200 operated at 200 kV acceleration voltage equipped with a GATAN OneView CMOS camera for fast imaging. Exposure conditions have been set in such a way, that the material does not alter by radiolysis during imaging.

For N_2 at 77 K, CO_2 at 195 K, and *n*-butane at 273 K adsorption measurements an Autosorb IQ apparatus from Quantachrome was used. Vapour physisorption measurements were carried out at 298 K at BELSORP-MAX of MicrotracBEL Corp. and the measuring routine of BELSORP-max control software was used. In general, equilibration conditions for each point were 1% pressure change within at least 300 s. For adsorption experiments below the standard boiling point of the adsorptive 1% within 500 s was set. The dead volume was routinely determined using helium. Values for the adsorbed amount of gas in the framework are all given at Standard Temperature and Pressure (STP). Prior to the measurements, the samples were activated in dynamic vacuum of 10 - 4 kPa at 373 K for at least 20 h to ensure complete removal of solvent molecules. For all adsorption measurements $Cu_2(dttc)_2$ (**2**) was used. Adsorption data are attached as SI as Standard Adsorption Information files (AIF).[1]

3. Experimental data

$[Cu_2(dttc)_2(L)_2(L)_x]_n$:

Synthesised and DMF-washed crystals of $[Cu_2(dttc)_2(DMF)_2(L)_x]_n$ were soaked in the excess of different solvents (2-heptanone, 2-propanol, 2-pentanone, acetone, butanone, ethanol, DMSO) over 14 d to exchange the original solvent molecules. The supernatant was replaced by the fresh one two times a day. The solvent exchanged crystals were subjected to single crystal X-ray analysis. The corresponding single crystal data are listed in Supplementary Tables 2-4.

$[Cu_2(dttc)_2]_n$:

After synthesis, the $[Cu_2(dttc)_2(DMF)_2(L)_x]_n$ crystals were suspended in fresh DMF, which was exchanged at least two times per day over a period of 5 d with anhydr. acetone. After that, the material was desolvated using supercritical CO_2.[2] For this purpose the MOF crystals, suspended in acetone, were transferred to sintered glass Buchner funnels and placed into a Jumbo Critical Point Dryer 13200J AB (SPI Supplies), which was subsequently filled with liquid CO_2 (99.995% purity) at 290 K and 6 MPa. To ensure a complete substitution of the solvent by CO_2, the liquid in the autoclave was exchanged with fresh CO_2 at least 15 times over 5 days using a valve at the bottom of the autoclave. The temperature and pressure were then risen beyond the supercritical point of CO_2 to 308 K and 10 MPa and kept until the temperature and pressure were constant. The supercritical CO_2 was released and the dry powder was transferred and stored in an argon-filled glove box.

Elemental analysis: Calculated ($Cu_2(dttc)_2$): C: 34.73%; H: 0.58%; N: 0%; S: 27.81%; found: C: 34.61%; H: 0.57%; N: 0%; S: 27.71%.

^{1}H NMR (300 MHz, DMSO-d_6/DCl): δ: 8.21 (s, 2H).

4. Theoretical calculations

The exfoliation of the ordered layered structure by energy input, such as ultrasonic treatment, undoubtedly results in the reorientation and rearrangement of the ligands in a certain way. Therefore, the linkers (benzene-1,4-dicarboxylic acid and dithieno[3,2-b:2',3'-d]thiophene-2,6-dicarboxylic acid) of the layered MOFs $[Cu_2(bdc)_2]_n$ and DUT-134 were considered in detail. Comprehensive sampling of the dimer conformations was investigated (Supplementary Figure 1). The simulations demonstrate the interactions of H_2bdc are much greater than H_2dttc, which is due to the curved structure of these molecules. Accordingly, the exfoliation should be improved for the bent ligand of DUT-134.

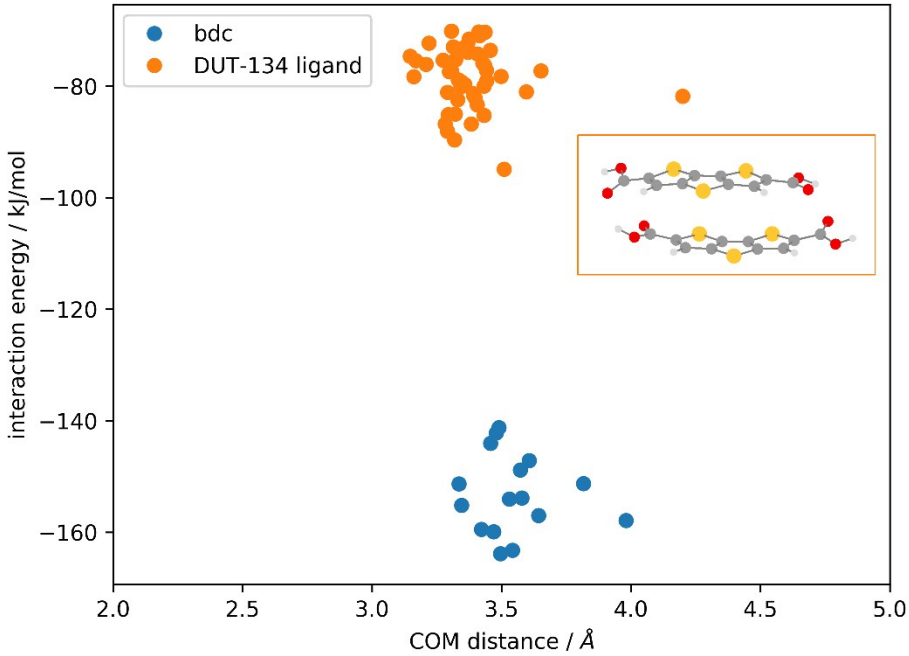

Supplementary Figure 1: The relative energy of dimer conformers identified by the CREST algorithm for the corresponding acids of bdc and dttc, with respect to their centre of mass (COM) distance.

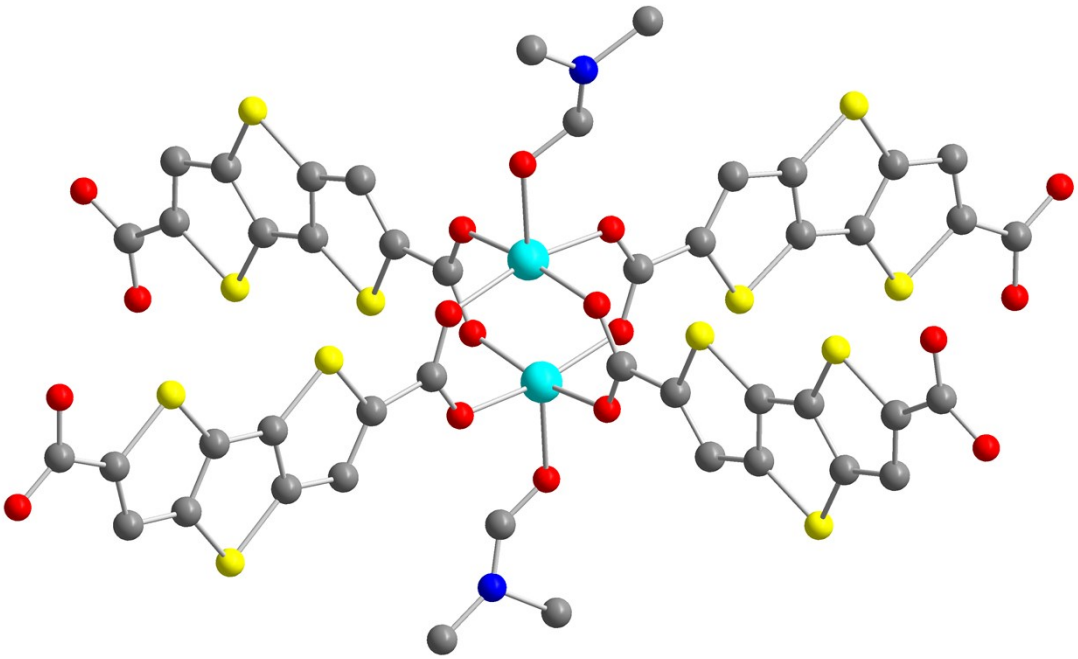

Supplementary Figure 3: Paddle wheel unit of DUT-134(Cu)·DMF. Color code: carbon (grey), nitrogen (blue), oxygen (red), sulfur (yellow), copper (cyan). Hydrogen atoms are omitted for clarity.

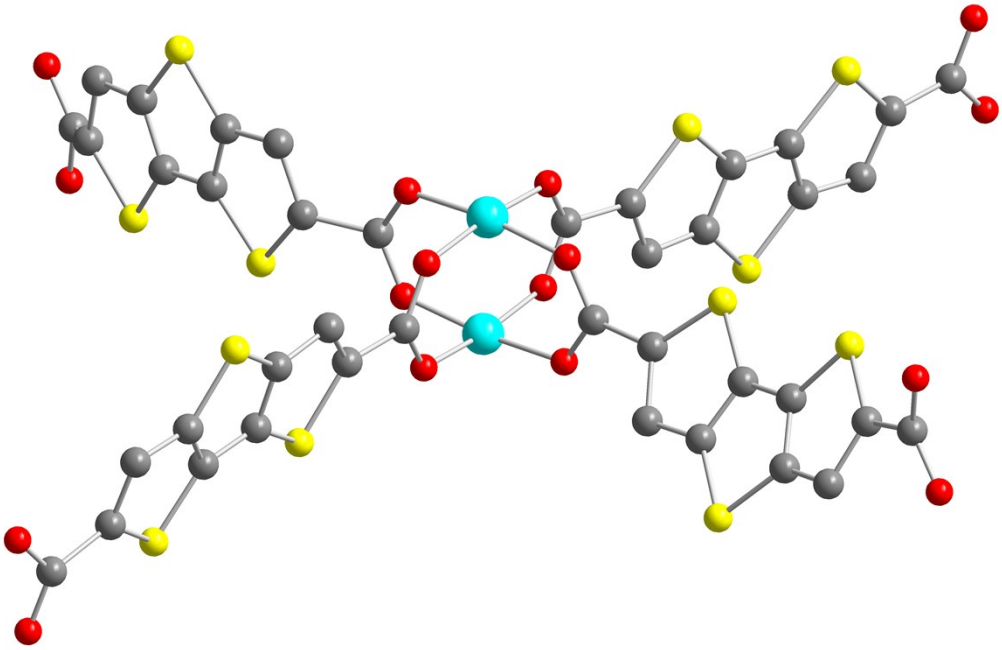

Supplementary Figure 2: Paddle wheel unit of DUT-134(Cu). Color code: carbon (grey), nitrogen (blue), oxygen (red), sulfur (yellow), copper (cyan). Hydrogen atoms are omitted for clarity.

5. Detailed crystallographic data

Supplementary Table 2: Single crystal data of DUT-134(Cu)·DMF, DUT-134(Cu)·DMSO and H_2dttc.

	DUT-134(Cu)·DMF	***DUT-134(Cu)·DMSO***	**H_2dttc**
Empirical formula	$C_{29}H_{25}Cu_2N_3O_{12}S_6$	$C_{24}H_{16}Cu_2O_{10}S_8$	$C_{10}H_4O_4S_3$
Formula weight	926.96	838.91	284.31
Wavelength, *Å*	0.7999	0.7999	0.71073
Crystal system, space group	Orthorhombic, *Pnma*	Orthorhombic, *Pnma*	Orthorhombic, *Pbcm*
Unit cell dimensions, *Å*	a = 17.880 (4)	a = 16.080 (3)	a = 3.7955(15)
	b = 27.930 (6)	b = 27.850 (6)	b = 10.979(5)
	c = 27.850 (6)	c = 27.940 (6)	c = 25.331(11)
Unit cell volume, *Å³*	13908 (5)	12512 (4)	1055.6(8)
Z	8	8	4
Absorption coefficient, *mm⁻¹*	1.14	1.344	0.699
***F*(000)**	3760	3365	576
θ range, °	1.16 – 30.00	1.16 – 28.07	3.22 – 26.49
Limiting indices	$-21 \leq h \leq 21$	$-18 \leq h \leq 18$	$-4 \leq h \leq 4$
	$-34 \leq k \leq 34$	$-32 \leq k \leq 29$	$-13 \leq k \leq 12$
	$-28 \leq l \leq 28$	$-27 \leq l \leq 28$	$-31 \leq l \leq 31$
Reflections collected / unique	175142 / 12759	67157 / 10084	7042 / 1106
R(int)	0.054	0.036	0.1458
Data / parameters	12759 / 476	10084 / 410	1106 / 84
GooF on F^2	1.060	1.357	1.144
Final *R* indices [$I>2\sigma(I)$]	R_1 = 0.0633	R_1 = 0.0984	R_1 = 0.1355
	wR_2 = 0.2217	wR_2 = 0.3307	wR_2 = 0.3666
R indices (all data)	R_1 = 0.0780	R_1 = 0.1087	R_1 = 0.1660
	wR_2 = 0.2427	wR_2 = 0.3604	wR_2 = 0.3845
Largest diff. peak / hole, eÅ⁻³	0.64 / -0.28	3.24 / -1.43	1.886 / -1.071
CCDC number	2069407	2069412	2069415

Supplementary Table 3: Single crystal data of DUT-134(Cu)·butanone, DUT-134(Cu)·acetone and DUT-134(Cu)·2-pentanone.

	DUT-134(Cu)·butanone	***DUT-134(Cu)·acetone***	***DUT-134(Cu)·2-pentanone***
Empirical formula	$C_{28}H_{20}Cu_2O_{10}S_6$	$C_{26}H_{16}Cu_2O_{10}S_6$	$C_{30}H_{24}Cu_2O_{10}S_6$
Formula weight	835.91	807.86	863.97
Wavelength, *Å*	0.7999	0.7999	0.7999
Crystal system, space group	Orthorhombic, *Pnma*	Orthorhombic, *Pnma*	Orthorhombic, *Pnma*
Unit cell dimensions, *Å*	a = 16.290 (3)	a = 16.190 (3)	a = 16.170 (3)
	b = 27.760 (6)	b = 27.770 (6)	b = 27.750 (6)
	c = 27.890 (6)	c = 27.870 (6)	c = 27.890 (6)
Unit cell volume, *Å³*	12612 (4)	12530 (4)	12515 (4)
Z	8	8	8
Absorption coefficient, 1/mm	1.24	1.25	1.25
***F*(000)**	3072	3248	3184
θ range, °	1.2 – 32.3	1.2 – 32.3	1.2 – 32.2
Limiting indices	$-21 \leq h \leq 21$	$-21 \leq h \leq 21$	$-21 \leq h \leq 21$
	$-31 \leq k \leq 31$	$-32 \leq k \leq 32$	$-36 \leq k \leq 36$
	$-37 \leq l \leq 37$	$-37 \leq l \leq 37$	$-31 \leq l \leq 31$
Reflections collected / unique	196611 / 14613	193018 / 14657	189993 / 14331
R(int)	0.066	0.074	0.061
Data / parameters	14613 / 400	14657 / 378	14331 / 378
GooF on F^2	1.064	1.072	1.074
Final R indices [$I>2\sigma(I)$]	R_1 = 0.0716	R_1 = 0.0651	R_1 = 0.0655
	wR_2 = 0.2117	wR_2 = 0.1991	wR_2 = 0.2001
R indices (all data)	R_1 = 0.0999	R_1 = 0.0964	R_1 = 0.0946
	wR_2 = 0.2495	wR_2 = 0.2355	wR_2 = 0.2377
Largest diff. peak / hole, eÅ^{-3}	1.81 / -0.50	1.46 / -0.65	1.33 / -0.54
CCDC number	2069408	2069413	2069411

Supplementary Table 4: Single crystal data of DUT-134(Cu)·EtOH, DUT-134(Cu)·2-PrOH and DUT-134(Cu)·2-heptanone.

	DUT-134(Cu)·EtOH	***DUT-134(Cu)·2-PrOH***	***DUT-134(Cu)·2-heptanone***
Empirical formula	$C_{24}H_{14}Cu_2O_{10}S_6$	$C_{26}H_{18}Cu_2O_{10}S_6$	$C_{34}H_{32}Cu_2O_{10}S_6$
Formula weight	781.82	809.87	920.07
Wavelength, *Å*	0.7999	0.7999	0.7999
Crystal system, space group	Orthorhombic, *Pnma*	Orthorhombic, *Pnma*	Orthorhombic, *Pnma*
Unit cell dimensions, *Å*	a = 15.580 (3)	a = 15.770 (3)	a = 15.830 (3)
	b = 27.680 (6)	b = 27.680 (6)	b = 27.710 (6)
	c = 27.830 (6)	c = 27.940 (6)	c = 27.880 (6)
Unit cell volume, *Å³*	12002 (4)	12196 (4)	12230 (4)
Z	8	8	8
Absorption coefficient, 1/mm	1.30	1.28	1.28
***F*(000)**	3136	3264	7980
θ range, °	1.17 – 28.14	1.17 – 28.03	1.17 – 32.24
Limiting indices	$-18 \leq h \leq 18$	$-18 \leq h \leq 18$	$-20 \leq h \leq 21$
	$-32 \leq k \leq 32$	$-32 \leq k \leq 32$	$-34 \leq k \leq 34$
	$-29 \leq l \leq 29$	$-29 \leq l \leq 29$	$-36 \leq l \leq 37$
Reflections collected / unique	127866 / 9710	133459 / 9893	179985 / 14989
R(int)	0.097	0.114	0.089
Data / parameters	9710 / 382	9893 / 400	14989 / 463
***GooF* on F^2**	1.060	1.087	1.042
Final *R* indices [*I>2σ(I)*]	R_1 = 0.0613	R_1 = 0.0731	R_1 = 0.0769
	wR_2 = 0.1761	wR_2 = 0.2238	wR_2 = 0.2252
***R* indices (all data)**	R_1 = 0.1202	R_1 = 0.1151	R_1 = 0.1281
	wR_2 = 0.2280	wR_2 = 0.2653	wR_2 = 0.2736
Largest diff. peak / hole, eÅ⁻³	0.47 / -0.70	1.11 / -0.44	1.58 / -0.44
CCDC number	2069410	2069416	2069409

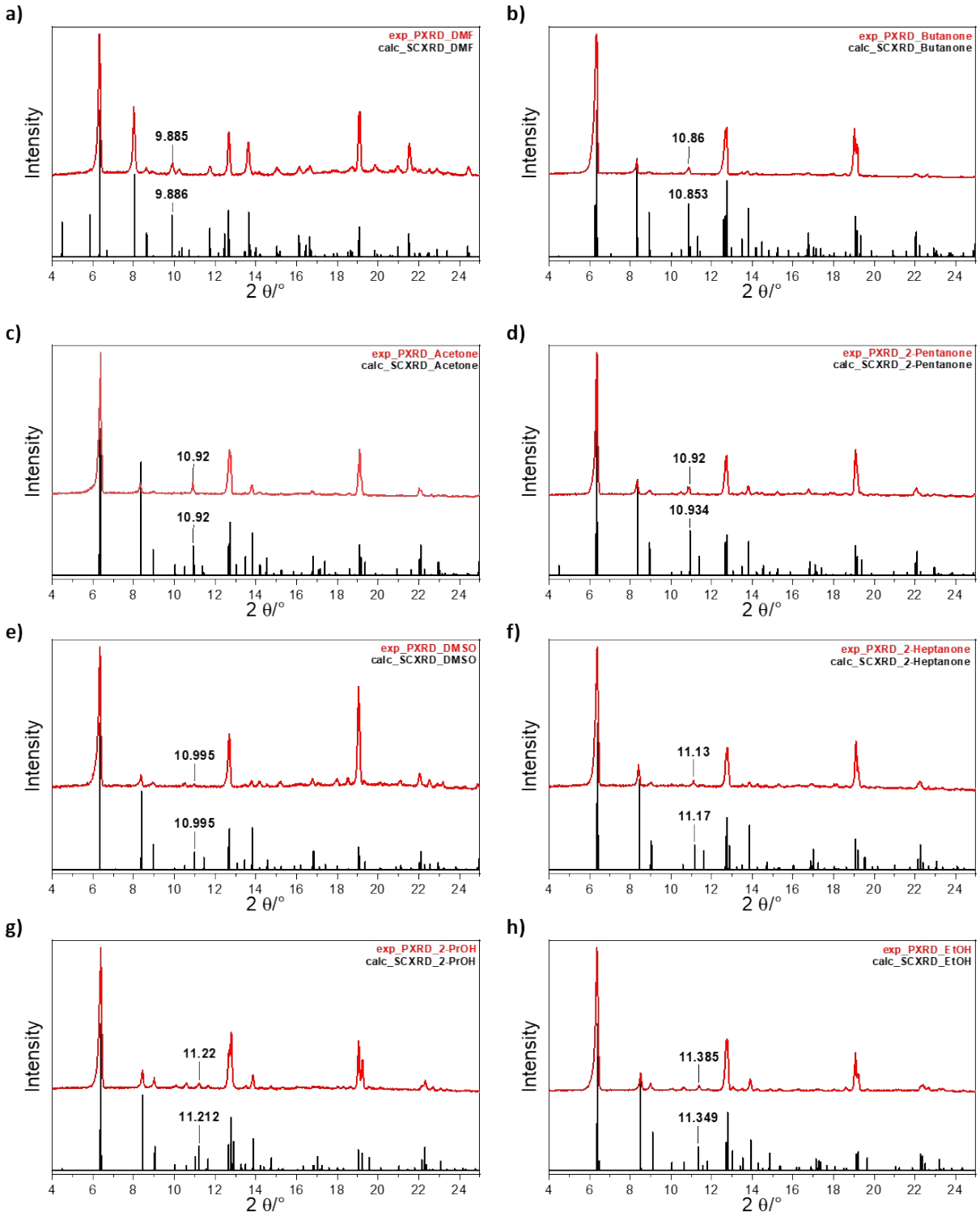

Supplementary Figure 4: Comparison of measured and theoretical PXRD patterns for compounds containing respective solvents: a) DMF, b) butanone, c) acetone, d) 2-pentanone, e) DMSO, f) 2-heptanone, g) 2-PrOH, h) EtOH.

6. Crystal structure of the dithieno[3,2-b:2',3'-d]thiophene-2,6-dicarboxylic acid (H_2DTTC)

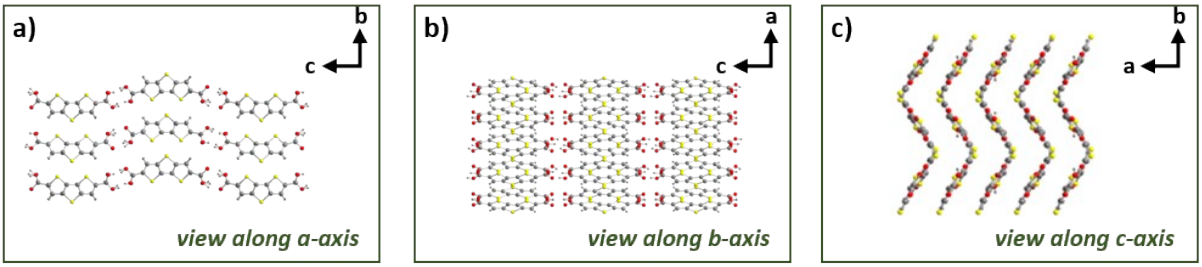

Supplementary Figure 5: Crystal structure of H_2dttc: a) view along *a*-axis; b) view along *b*-axis; c) view along *c*-axis.

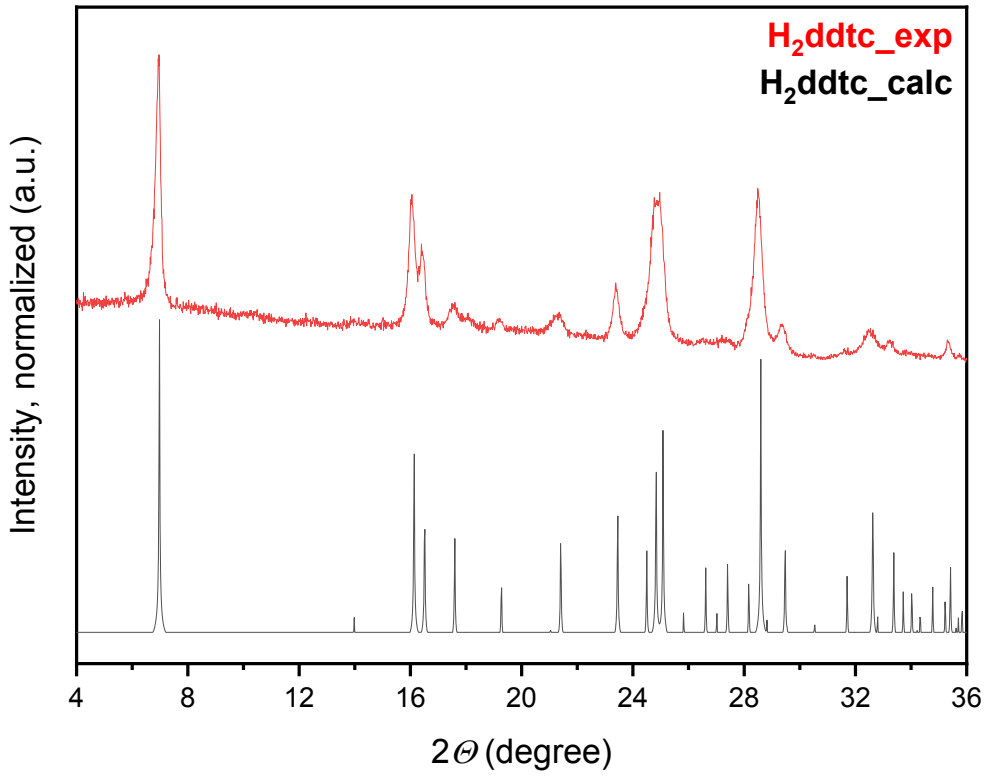

Supplementary Figure 6: Comparison of experimental (red) and theoretical (black) powder X-ray diffraction patterns of H_2dttc.

7. Optical and SEM images

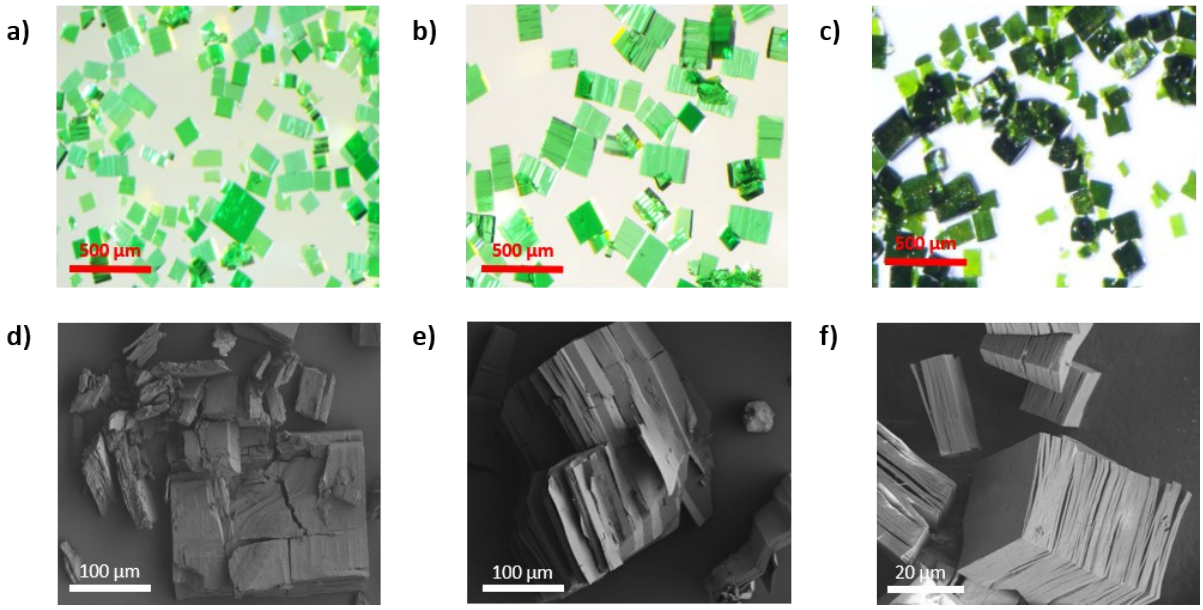

Supplementary Figure 7: Light microscope images of DUT-134: a) in DMF (as made), b) after solvent exchange to acetone, c) supercritically dried from acetone. Samples shown in a) and b) were dried in dynamic vacuum at 150 °C and measured by SEM. The corresponding images are shown in d) and e), respectively. The supercritically dried samples were prepared in the glove box using a sample holder designed for sample transfer under *inert gas. The* SEM image is shown in (f).

8. Comparison of different activation methods

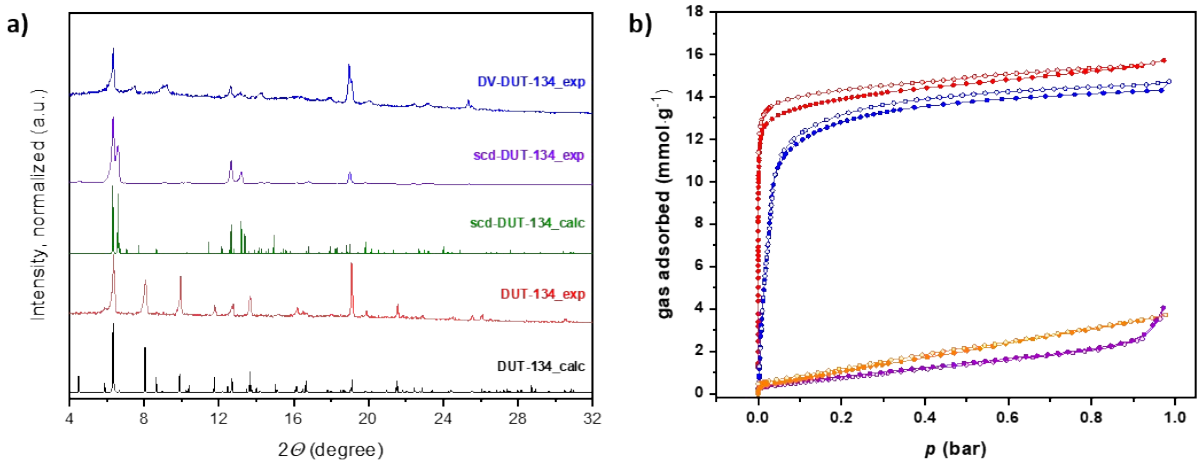

Supplementary Figure 8: a) XRD patterns of DUT-134 compound: "as made" $[Cu_2(DTTC)_2(DMF)_2(L)_x]_n$ - in red, activated by dynamic vacuum at 150 °C from DMF - in blue, and dried with supercritical CO_2 - purple. The theoretical XRD patterns calculated for DUT-134·DMF $[Cu_2(DTTC)_2(DMF)_2]_n$ (**1**) is shown in black (the solvent molecules in the pores (L) could not be localised in the crystal structure), and the theoretical XRD patterns calculated for DUT-134 $[Cu_2(DTTC)_2]_n$ (**2**) is shown in green; b) Nitrogen physisorption isotherms at 77 K performed on supercritically dried (SCD) DUT-134 sample (red), on DUT-134 dried in dynamic vacuum at 150 °C from DMF (purple), and on DUT-134 dried in dynamic vacuum at 150 °C from acetone (orange). The CO_2 physisorption isotherms at 195 K of SCD dried sample are shown in blue. Solid symbols – adsorption, open symbols – desorption.

9. High-resolution TEM measurements

HRTEM image processing and FT analysis were performed using DigitalMicrograph software by Gatan Inc., USA.[3]

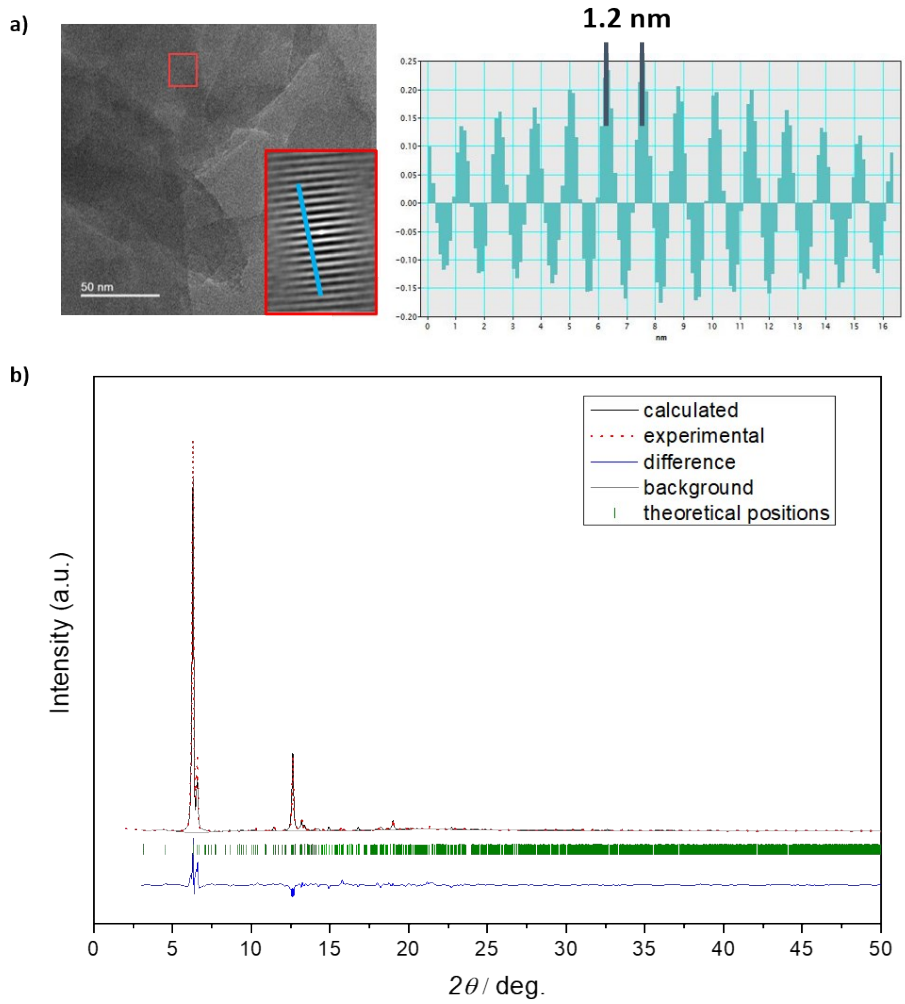

Supplementary Figure 9: a) HRTEM image of DUT-134(Cu) (**2**) crystals (left) as well as FT analysis (right) and intensity profiles of region marked in red in the HRTEM image; b) Rietveld refinement plot.

10. Adsorption isotherms

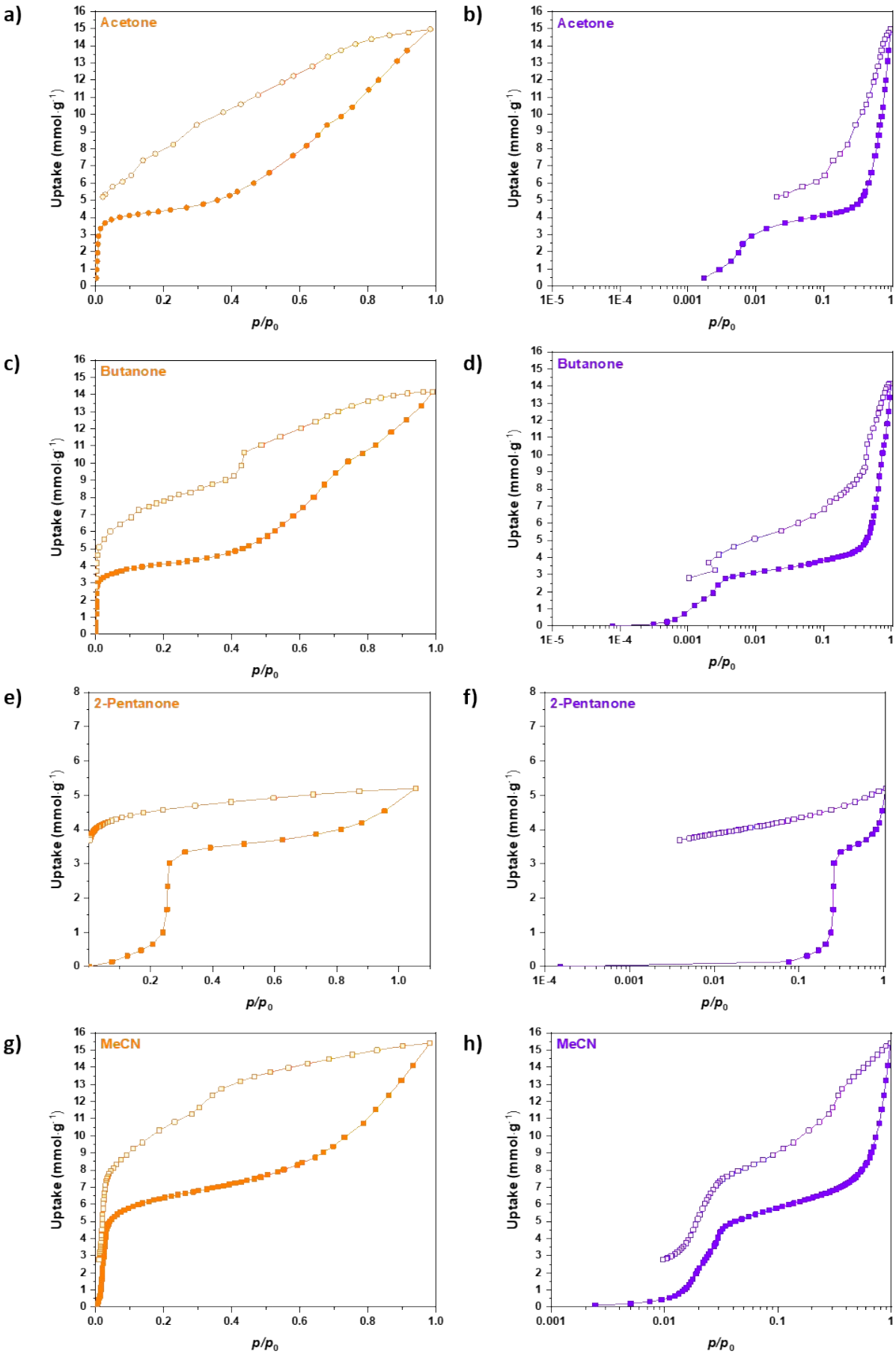

Supplementary Figure 10: Physisorption isotherms at 289 K for different vapours and their respective semi-logarithmic plots; a), b) acetone (p_0 = 30.7 kPa); c), d) butanone (p_0 = 12.06 kPa); e), f) 2-pentanone (p_0 = 4.70 kPa); g), h) MeCN (p_0 = 11.87 kPa).

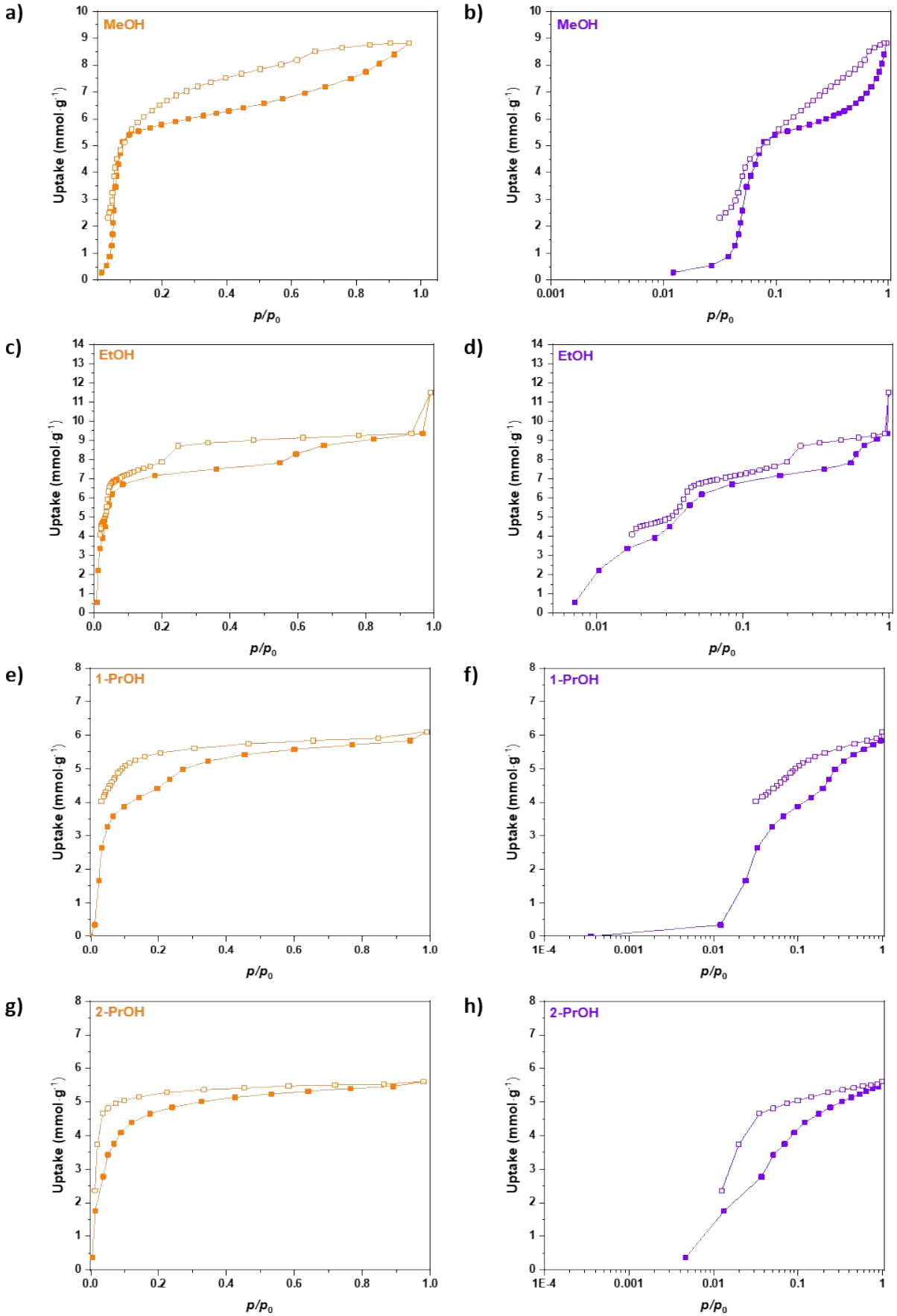

Supplementary Figure 11: Physisorption isotherms at 289 K for different solvents and their respective logarithmic plots; a), b) MeOH (p_0 = 16.80 kPa); c), d) EtOH (p_0 = 7.87 kPa); e), f) 1-PrOH (p_0 = 3.10 kPa); g), h) 2-PrOH (p_0 = 5.79 kPa).

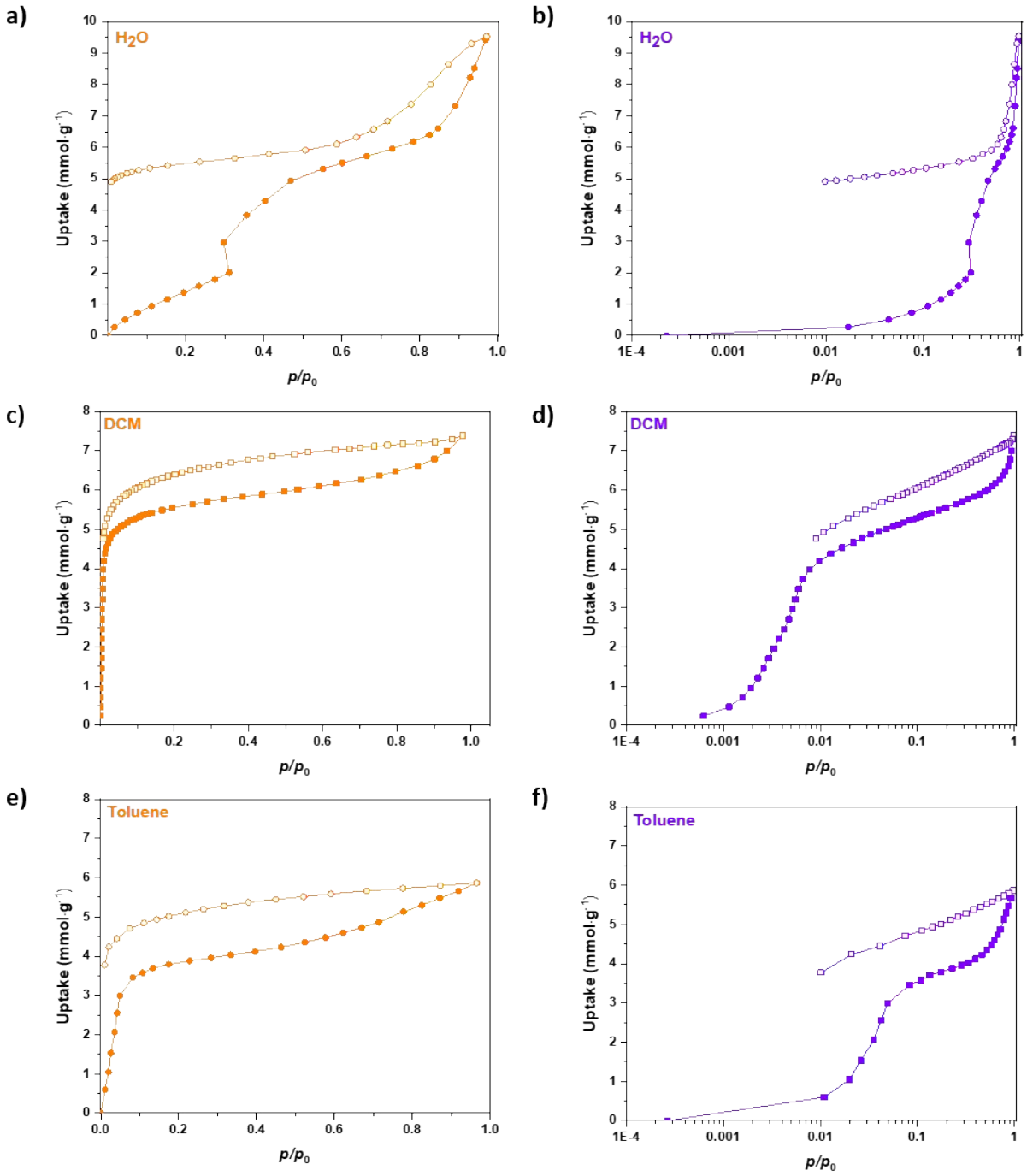

Supplementary Figure 12: Physisorption isotherms at 289 K for different vapors and their respective semi-logarithmic plots; a), b) H_2O (p_0 = 3.14 kPa); c), d) dichlormethane (p_0 = 57.38 kPa); e), f) toluene (p_0 = 3.82 kPa).

11. Zeo++ calculations[4]

Supplementary Table 5: Adsorptive and porosity characteristics.

Adsorptive	Kinetic radius [Å]	Molar mass [g/mol]	Density [g/cm³]	POAV (Zeo++) [cm³/g]	Expected uptake based on cryst. data [mmol/g]	Exp. pore volume [cm³/g]	Exp. uptake [mmol/g]
CO_2	1.70	44.01	1.56	0.50	17.56	0.44	15.70
N_2	1.82	28.00	0.807	0.49	14.07	0.50	14.30
***n*-Butane**	2.34	58.12	0.6	0.46	4.47	0.51	5.30
Acetone	2.24	58.08	0.784	0.46	6.23	1.11	14.95
Butanone	2.60	72.11	0.805	0.44	4.93	1.27	14.15
2-Pentanone	2.70	86.13	0.81	0.44	4.10	0.48	4.53
MeOH	1.90	32.04	0.792	0.48	11.92	0.36	8.81
EtOH	2.25	46.07	0.789	0.46	7.90	0.55	9.37
1-PrOH	2.25	60.1	0.803	0.46	7.90	0.46	6.10
2-PrOH	2.40	60.1	0.786	0.45	5.93	0.44	5.80
MeCN	3.26	41.05	0.78	0.41	7.74	0.81	15.41
H_2O	1.48	18.00	1.00	0.52	28.87	0.17	9.54
Toluene	2.90	92.14	0.876	0.43	4.05	0.57	5.87
DCM	2.30	84.93	1.33	0.46	7.19	0.47	7.39

POAV - accessible probe-occupiable volume

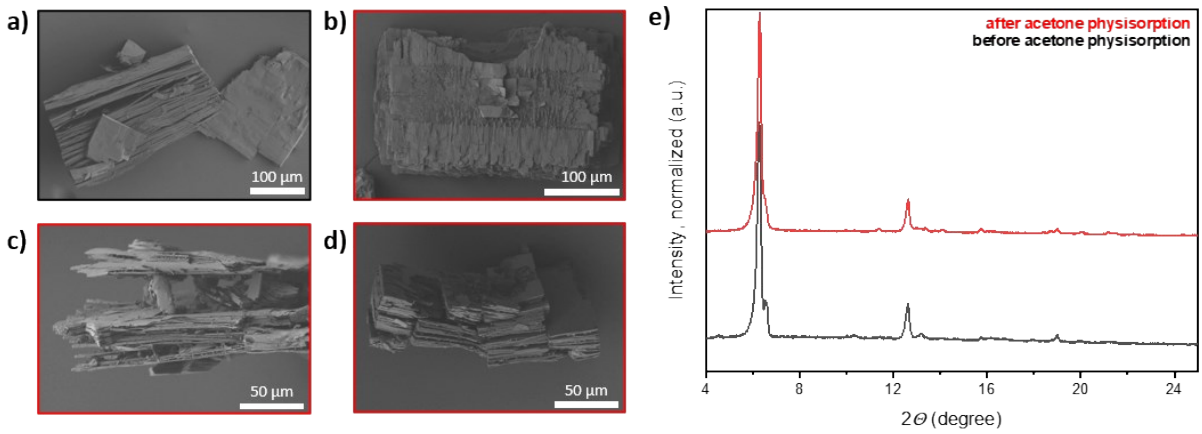

Supplementary Figure 13: SEM images of DUT-134(Cu) before (a) and after (b), (d) and (c) physisorption of acetone; e) PXRD patterns of a sample before and after physisorption measurement.

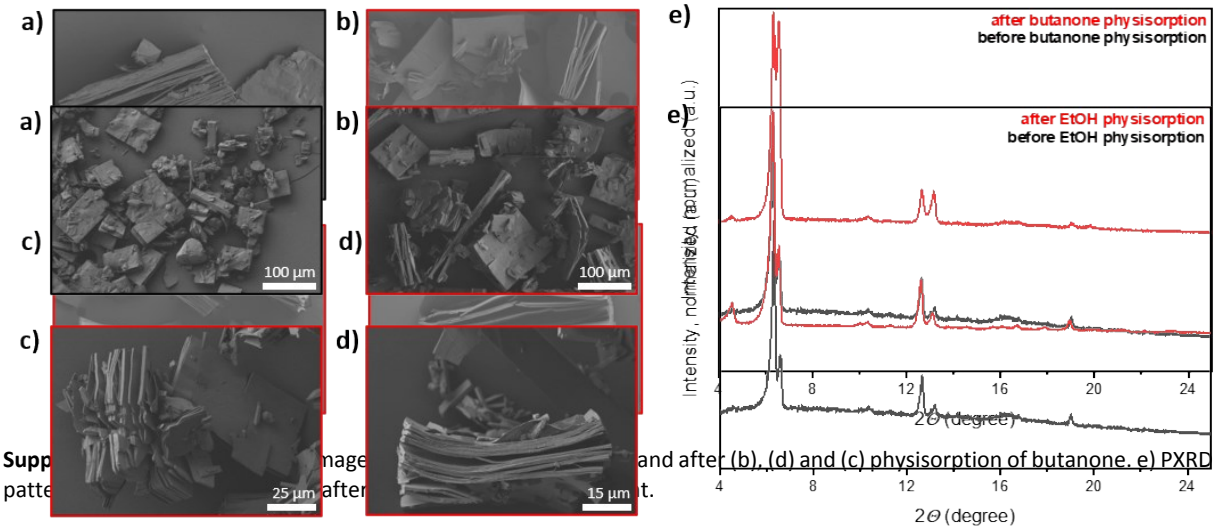

Supp mage and after (b), (d) and (c) physisorption of butanone. e) PXRD patte after t.

Supplementary Figure 15: SEM data of DUT-134(Cu) before (a) and after (b), (d) and (c) physisorption of ethanol; e) PXRD patterns of a sample before and after physisorption measurement.

12. In situ PXRD during *n*-butane adsorption at 273 K

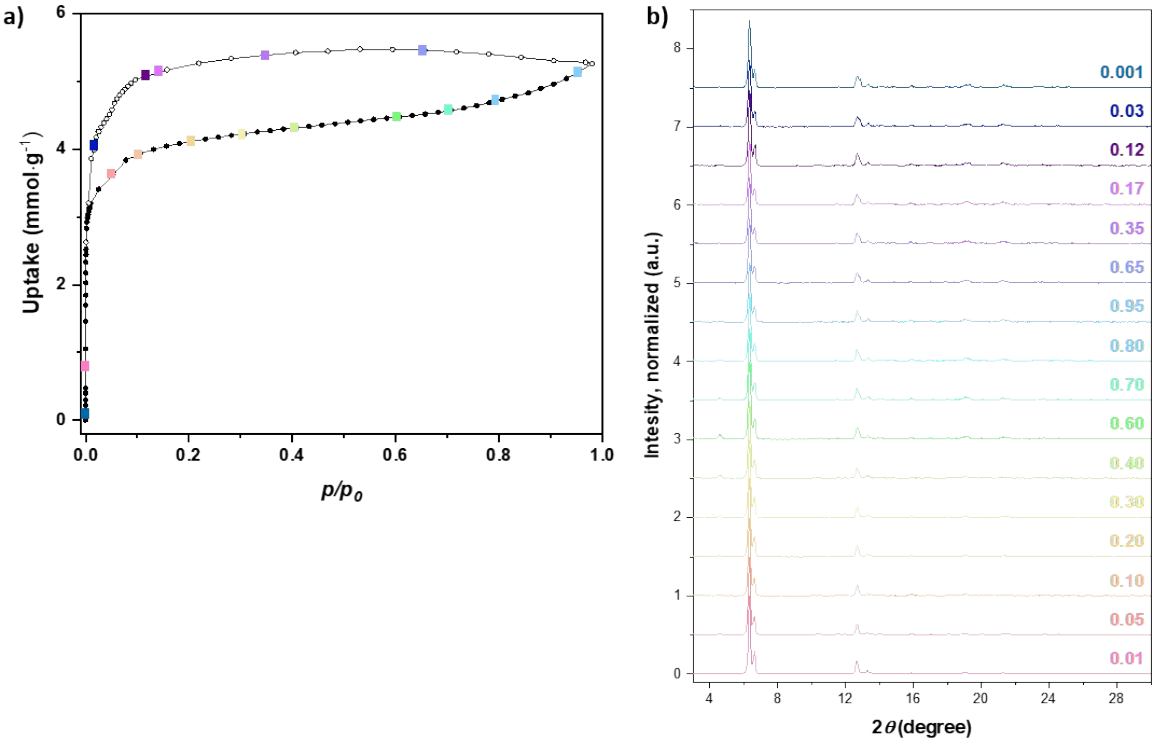

Supplementary Figure 16: Combined *n*-butane physisorption and PXRD measurements: a) *n*-butane physisorption isotherm measured ex situ at 273 K. The pressure points, which correspond to the collected XRD patterns are marked by colored circles; b) PXRD patterns collected after appropriate equilibration in the adsorption points at corresponding relative pressures highlighted close to the XRD patterns.

13. Ex situ PXRD during EtOH adsorption at 298 K

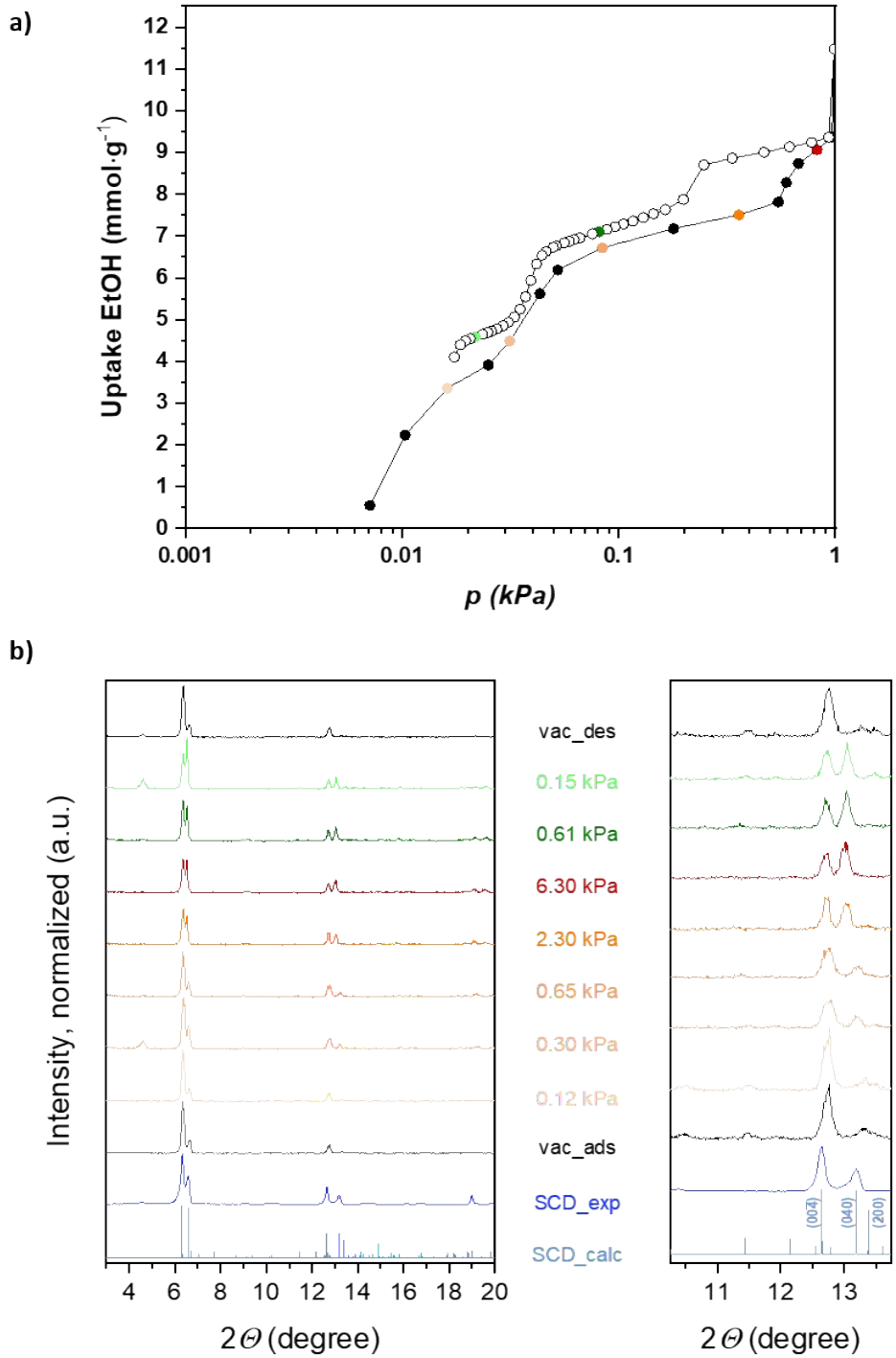

Supplementary Figure 17: Combined EtOH physisorption and PXRD measurements: a) EtOH vapor physisorption isotherm measured ex situ at 298 K. The pressure points, which correspond to the collected XRD patterns are marked by colored circles; b) PXRD patterns collected after appropriate equilibration in the adsorption points at corresponding relative pressures highlighted close to the XRD patterns.

14. Exfoliation

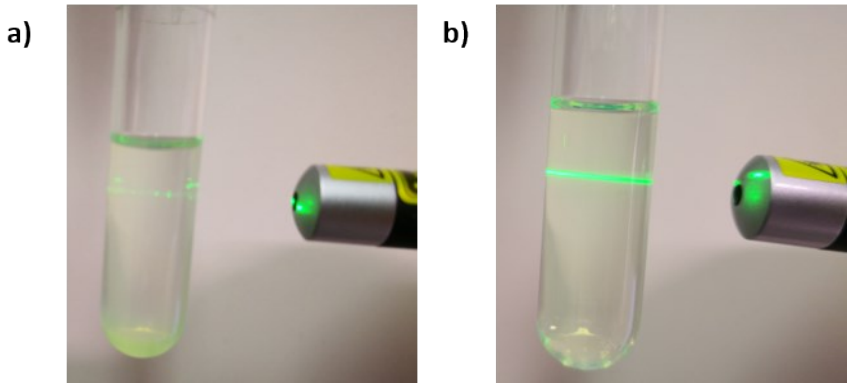

Supplementary Figure 18: Comparison of Rayleigh scattering after 24 h ultrasound treatment a) in DMF; b) in butanone.

From the sediment visible in image (a), it can be concluded that the particles in DMF agglomerate (reassemble) with time. Therefore, DMF is not suitable to obtain stable suspensions. The long-term stability of the suspension is improved in butanone or acetone.

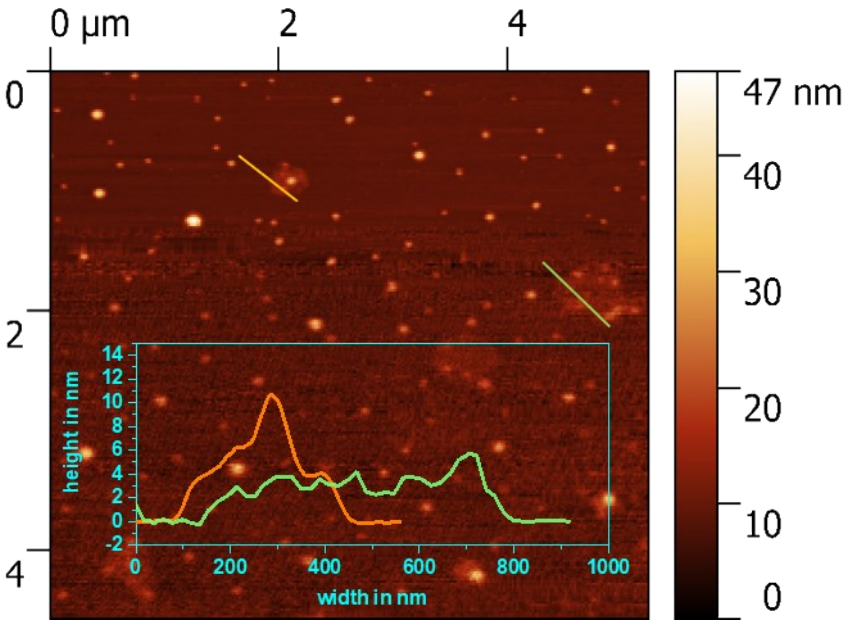

Supplementary Figure 19: AFM image of particles obtained by ultrasonication (30 s) in butanone.

15. Thermogravimetric analysis

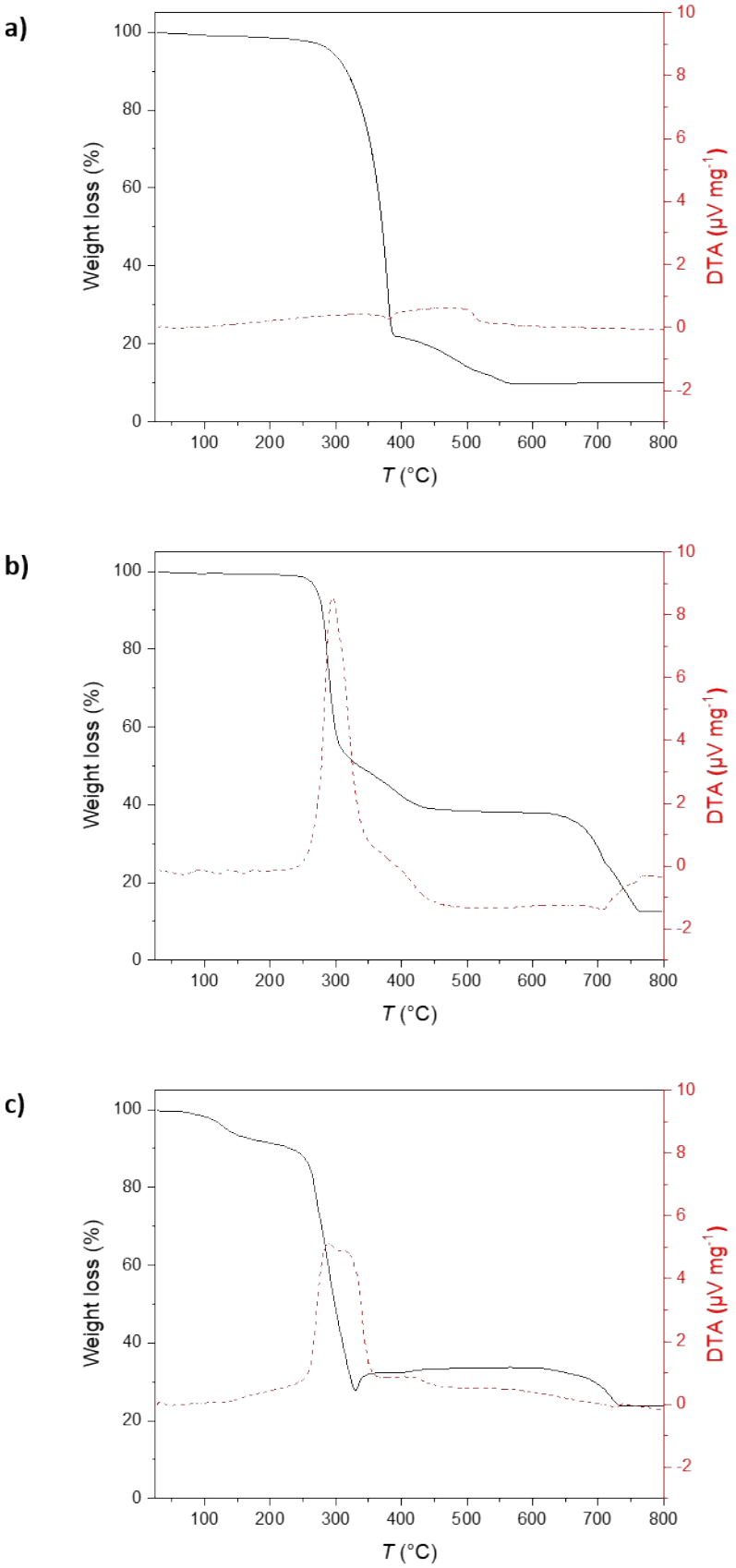

Supplementary Figure 20: Thermogravimetric analysis of: a) H_2dttc; b) $[Cu_2(dttc)_2]_n$; c) $[Cu_2(dttc)_2(DMF)_2(L)_x]_n$.

16. Infrared (IR) and Raman spectroscopy

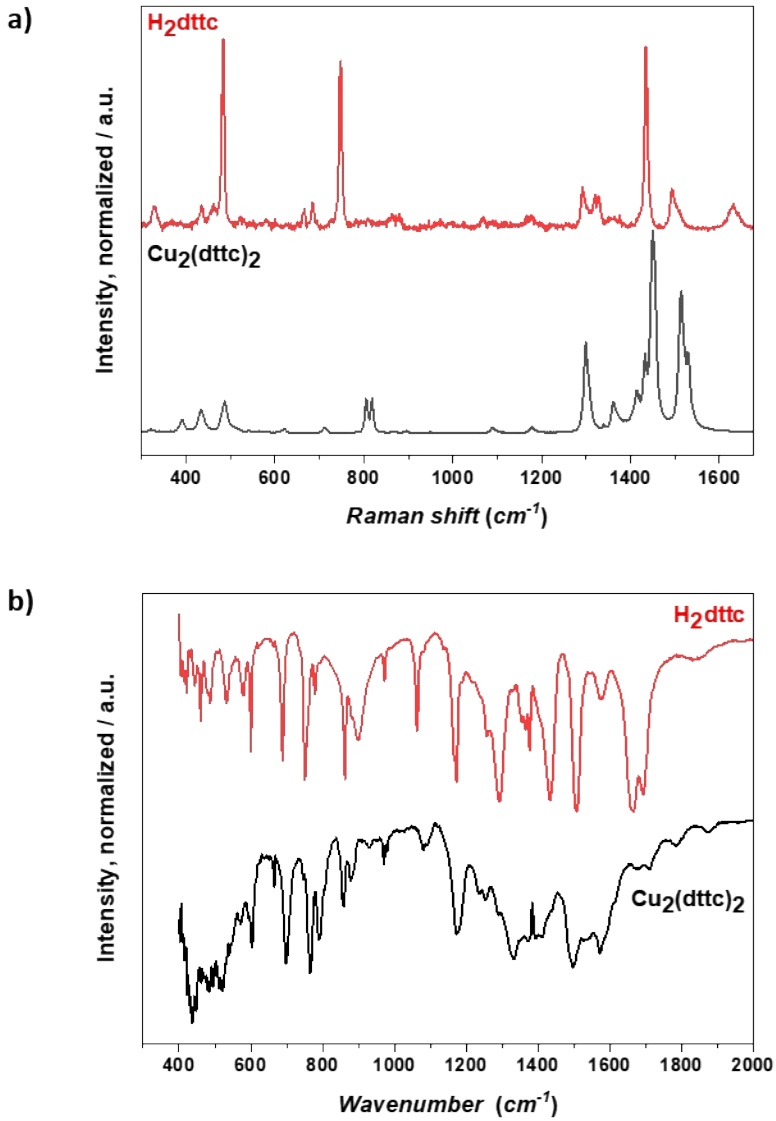

Supplementary Figure 21: a) Raman spectra of H_2dttc (red) and $[Cu_2(dttc)_2]_n$ (black), b) IR spectra H_2dttc (red) and $[Cu_2(dttc)_2]_n$ (black).

17. NMR spectroscopy

a)

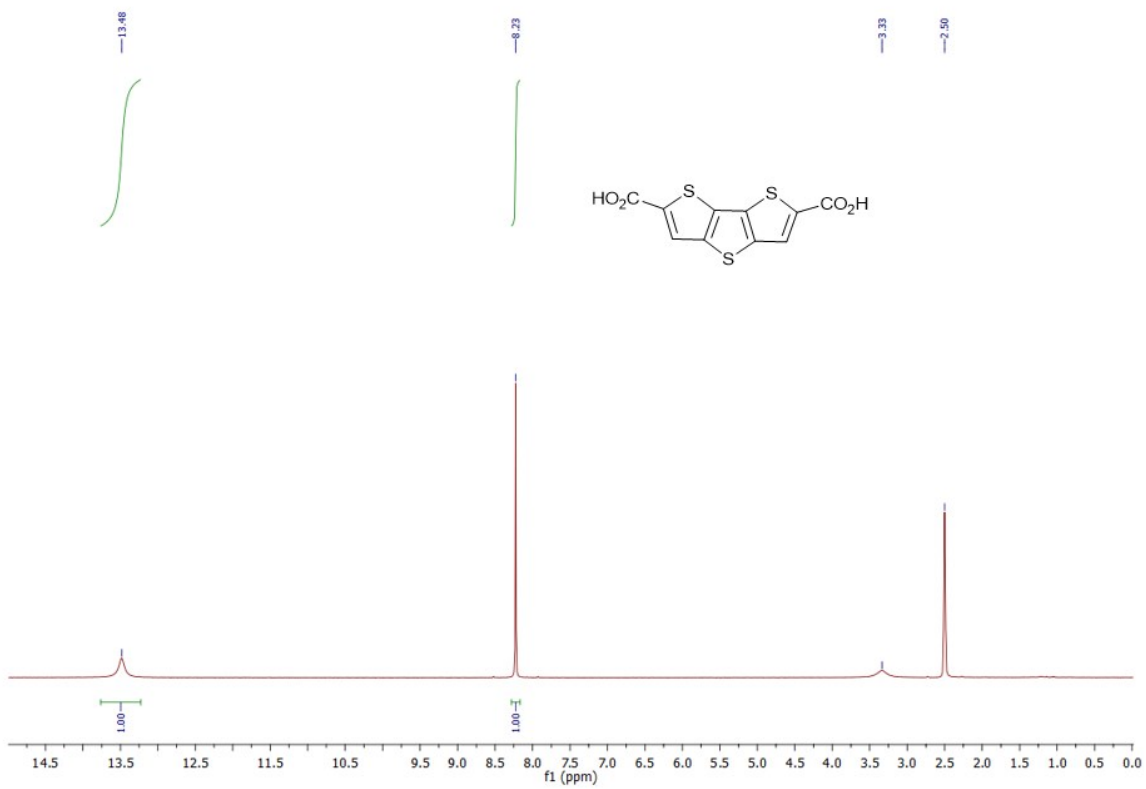

b)

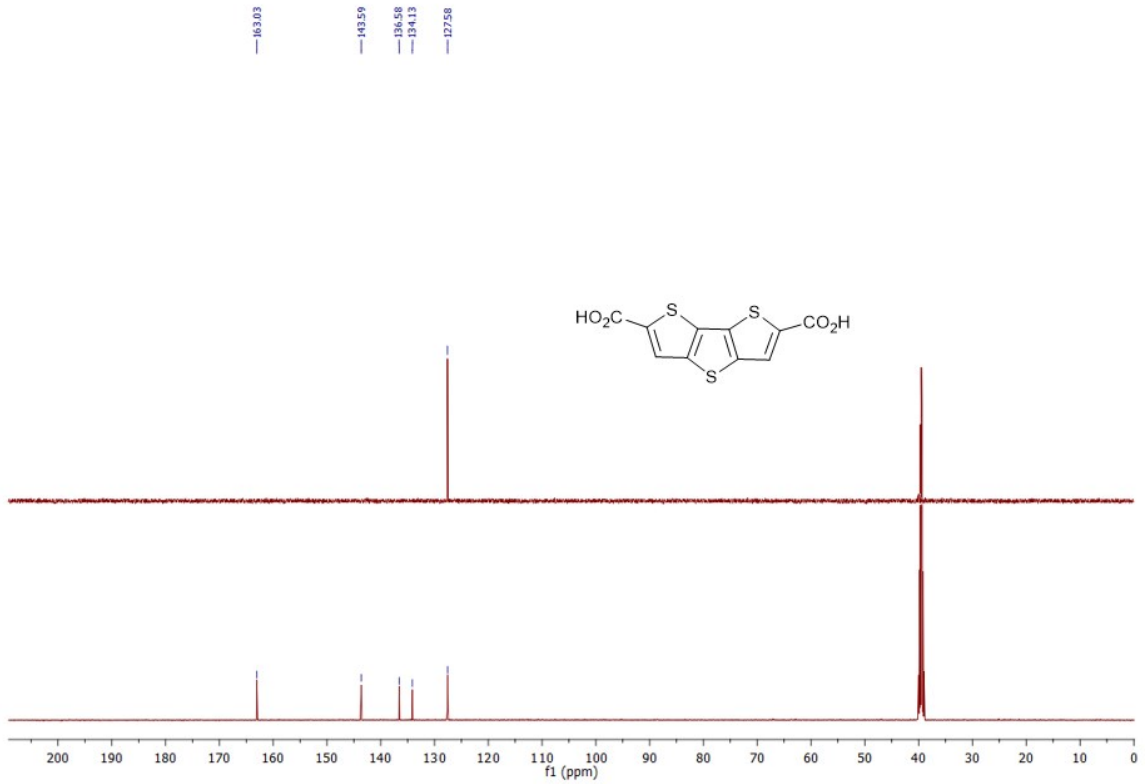

Supplementary Figure 22: NMR spectra of H_2dttc: a) ^{1}H NMR (500 MHz) in DMSO-d_6, b) ^{13}C NMR (126 MHz) in DMSO-d_6.

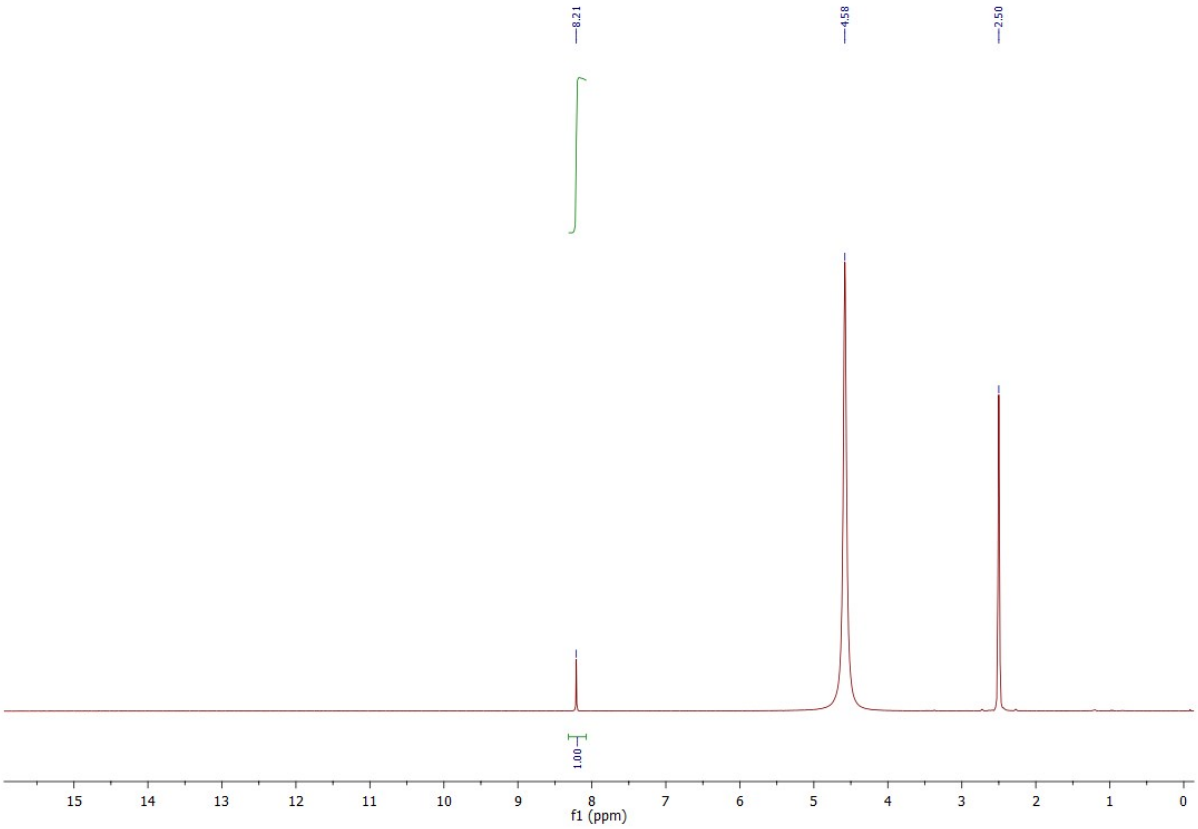

Supplementary Figure 23: ^{1}H NMR spectra of $[Cu_2(dttc)_2]_n$ digested in DCl/DMSO-d6 after supercritical drying. No solvents (neither DMF nor acetone) are present in the pores of the framework, in agreement with the elemental analysis data.

References

1. J. D. Evans, V. Bon, I. Senkovska and S. Kaskel, A universal standard archive file for adsorption data, *Langmuir*, 2021, **37**, 4222–4226.
2. R. Grünker, V. Bon, P. Müller, U. Stoeck, S. Krause, U. Mueller, I. Senkovska and S. Kaskel, A new metal–organic framework with ultra-high surface area, *Chem. Commun.*, 2014, **50**, 3450-3452.
3. Gatan Microscopy Suite 3, Gatan Inc., Pleasanton, California, USA.
4. T. F. Willems, C. H. Rycroft, M. Kazi, J. C. Meza and M. Haranczyk, Algorithms and tools for high-throughput geometry-based analysis of crystalline porous materials, *Microporous Mesoporous Mat.*, 2012, **149**, 134-141.